applied sciences

MDPI

Article

Urban-Scale Dynamic Screening for the Preliminary Seismic-Risk Prioritization of Masonry Buildings

Marco Gatti

Department of Engineering, University of Ferrara, Via Saragat 1, 44122 Ferrara, Italy; marco.gatti@unife.it

Abstract

This paper proposes an urban-scale dynamic screening method for the preliminary seismic-risk prioritization of masonry buildings. The method is based on the integration of rapid surveys, relational databases, geographic information systems, and accelerometric data recorded during seismic events. It is not intended to replace comprehensive seismic vulnerability or risk assessment procedures. In its present formulation, it provides an event-specific preliminary dynamic-priority indicator, derived from recorded ground motions, to support post-event inspections and subsequent detailed analyses at the urban scale. The procedure combines a rapid visual survey (on average covering ca. 300 buildings per day) with a database management system (DBMS) linked to a three-dimensional cartographic database of the building stock. The geometric and structural information collected in the field is integrated with the processing of ground acceleration records, from which the pseudo-acceleration spectra, peak ground acceleration (PGA), and spectral amplification ratios (DAF) are derived. Through the relationship between spectral period and building height, the method identifies height classes and number of storeys corresponding to the highest spectral amplification ratios derived from the recorded ground motions. Buildings belonging to these classes are not classified as vulnerable in absolute terms, but are considered priority buildings for subsequent checks, inspections, or detailed analyses. The method was applied to the municipalities of Umbertide and Gubbio, in the province of Perugia, which were affected by the seismic sequence of 9 March 2023. The processed accelerometric records identified Classes I, II and III, corresponding to one-, two-, and three-storey masonry buildings. The illustrative GIS application focused on Classes II and III; 27 of the 33 masonry buildings included in the damaged-building sample (82%) belonged to these two classes. The main contribution of the study is the definition of an integrated, rapid, and replicable workflow that can support local authorities, technicians, and civil protection operators in the preliminary management of seismic risk at the urban scale.

Keywords: dynamic screening; seismic risk; masonry buildings; rapid visual survey; relational databases; GIS; spectral amplification ratio; urban scale

Check for updates

Academic Editor: Sang-Hyo Kim

Received: 12 July 2026
Revised: 12 August 2026
Accepted: 13 August 2026
Published: 19 August 2026

Copyright: © 2026 by the author. Licensee MDPI, Basel, Switzerland. This article is an open access article distributed under the terms and conditions of the Creative Commons Attribution (CC BY) license.

1. Introduction

Estimation of the seismic risk of masonry buildings based on numerical calculation requires long and laborious computational processes. Therefore, except for estimations of single units or for buildings that cannot be exposed to earthquakes [1,2], simplified estimation methods have been elaborated, especially in areas characterized by complex tectonic scenarios [3–5]. These rapid procedures [6–9], indicated in the literature by the acronym RVS (rapid visual screening), have been applied in Italy [10], Albania [11], Algeria [12,13],

Bosnia [14], Canada [15,16], Japan [17], Greece [18–21], Indonesia [22], New Zealand [23], India [24], Thailand [25–27], the Philippines [28], Turkey [29–31], and Taiwan [32]. Their importance, in terms of applications and results, has been further consolidated with the advent of "soft computing" techniques, such as artificial neural networks [33–38], fuzzy logic [39,40], machine learning [41–43], and probabilistic approaches [44], both in their classic and revised formulations [45–49].

Some RVS methods have been related to the period of construction, others to the masonry type or to the presence of damage mechanisms [50–54], and others to the geometry of the building [55–57], for both high-magnitude earthquakes [58–61] and moderate ones [62–65].

Because of their nature, these methods have been supported by geographic information systems (GISs) [66–81], creating a synergy between geometric information storage, territorial data management, and preliminary seismic risk analysis. This integration is particularly useful when the information collected in the field must be organized into queryable databases and represented cartographically at the urban or territorial scale.

The recent devastating earthquake in Turkey [82] highlighted how many masonry buildings had been built without respecting the most basic anti-seismic design standards [83–85] and were therefore vulnerable also in relation to their geometric configuration. For this reason, it seemed appropriate to enrich RVS methods by proposing a preliminary dynamic-screening approach.

The method enables seismic-risk prioritization maps to be produced for masonry buildings whose heights or number of storeys correspond to the highest spectral amplification ratios derived from the ground motions recorded in the study area after the earthquake.

These buildings are not considered vulnerable in absolute terms, but are identified as buildings to be regarded as priorities for subsequent checks, inspections, or detailed analyses.

In this framework, building geometry, particularly height or number of storeys above ground, is not considered an exhaustive indicator of seismic vulnerability. It nevertheless provides a useful parameter for preliminary screening, since it allows the spectral characteristics of the recorded ground motion to be related to the height classes of the building stock through the empirical period-height relationship.

The method initially involves a rapid survey of the masonry building stock to collect geometric data, including height and number of storeys above ground, together with information on the principal construction and structural characteristics. The survey can be carried out using handheld devices, such as PDAs or tablets, equipped with digital cartography, spreadsheet software, and a photographic device. The operator identifies each building on the map and records geometric, historical, material, and structural information in pre-compiled digital tables. Data entry is accelerated through alphanumeric lists and data dictionaries accessible via drop-down menus.

The content of the survey is transferred to a dedicated information system consisting of a relational database management system (DBMS) and a cartographic database of two-dimensional polygons of the building stock; the latter are converted into three-dimensional representations by associating the building height or number of storeys above ground recorded during the survey.

Subsequently, the acceleration records acquired in the study area after an earthquake are obtained from the national seismic networks and processed to calculate the pseudo-acceleration spectra and the corresponding spectral amplification ratios. By combining this event-specific spectral indicator with the empirical period-height relationship, the building height classes associated with the highest spectral amplification ratios are identified.

At this point, the masonry buildings are reported in a GIS with a three-dimensional cartographic database, and those with heights or number of storeys corresponding to the highest spectral amplification ratios derived from the recorded ground motions are selected and mapped.

They are classified, from a geometric and dynamic point of view, as buildings to be regarded as priorities in a preliminary phase of seismic-risk analysis, and not as buildings vulnerable in absolute terms.

The method was tested in an area comprising some municipalities in the province of Perugia subject to frequent earthquakes [86], following the last event of 9 March 2023. A rapid survey yielded geometric information, with particular reference to height and structural data, with an average production of ca. 300 buildings/day. In the same area, accelerometric recordings of the above-mentioned earthquake were available from the stations of the Civil Protection seismic network and the National Institute of Geophysics and Volcanology. The corresponding spectral amplification ratios were calculated and related to building height through the empirical period-height relationship, thereby obtaining maps of the buildings to be regarded as priorities for subsequent checks.

The damage caused by the same earthquake to some buildings was also recorded during the survey, and the data were then used for a preliminary application-based verification of the method.

The availability of versatile instrumentation for rapid field surveys, regional cartographic databases of the building stock, and numerous accelerometric recording stations makes the proposed method a practical event-specific tool for post-earthquake screening and preliminary prioritization. Its possible preventive application would require the use of representative or design-level spectra and is not evaluated in the present study.

2. The Method

2.1. Method Overview

The method identifies and maps, in an event-specific post-earthquake screening phase, masonry buildings whose height, or number of storeys above ground, corresponds to the highest spectral amplification ratios derived from the recorded ground motions. The resulting classification represents a preliminary dynamic-priority indicator and not a complete assessment of seismic risk or structural vulnerability.

The first phase consists of a rapid visual survey (RVS) of the geometric information, including height, and structural information of the masonry buildings. The survey is mainly carried out visually from the outside of the building and in a rapid manner; therefore, the acquired information and the corresponding annotations are recorded in tables whose fields are structured with attributes that exhaustively describe the geometric-structural information and, at the same time, can be easily completed on a spreadsheet through drop-down menus (data dictionaries).

The second phase consists of identifying the accelerometric recording stations located in the study area and obtaining the ground-acceleration records acquired during the seismic event. The accelerograms are processed to calculate the pseudo-acceleration spectra and the corresponding spectral amplification ratios as functions of the oscillator period.

The third phase relates the highest spectral amplification ratios derived from the recorded ground motions to building height, thereby identifying the height classes to be regarded as priorities for subsequent inspections or detailed analyses.

The method requires basic numerical cartography both to identify the building during the survey and in the map creation phase. This is taken from 2D digital maps, at an urban scale and in vector format, available online in the regional topographic databases (DBT),

which, when integrated with the building height data recorded during the survey, make it possible to obtain the 3D database.

Finally, the information acquired during the previous phases is managed and queried through a DBMS using structured query language (SQL). The DBMS is linked to an open-source GIS used to map the resulting dynamic-priority classes of the masonry building stock.

The method shown in Figure 1 comprises three main phases: (i) rapid visual survey and structuring of the geometric, structural, and damage data; (ii) processing of the recorded ground accelerations to relate the dynamic response to building height and identify the height classes assigned higher dynamic priority; and (iii) integration of the survey data, DBMS, DBT, SQL queries, and GIS to map the selected buildings.

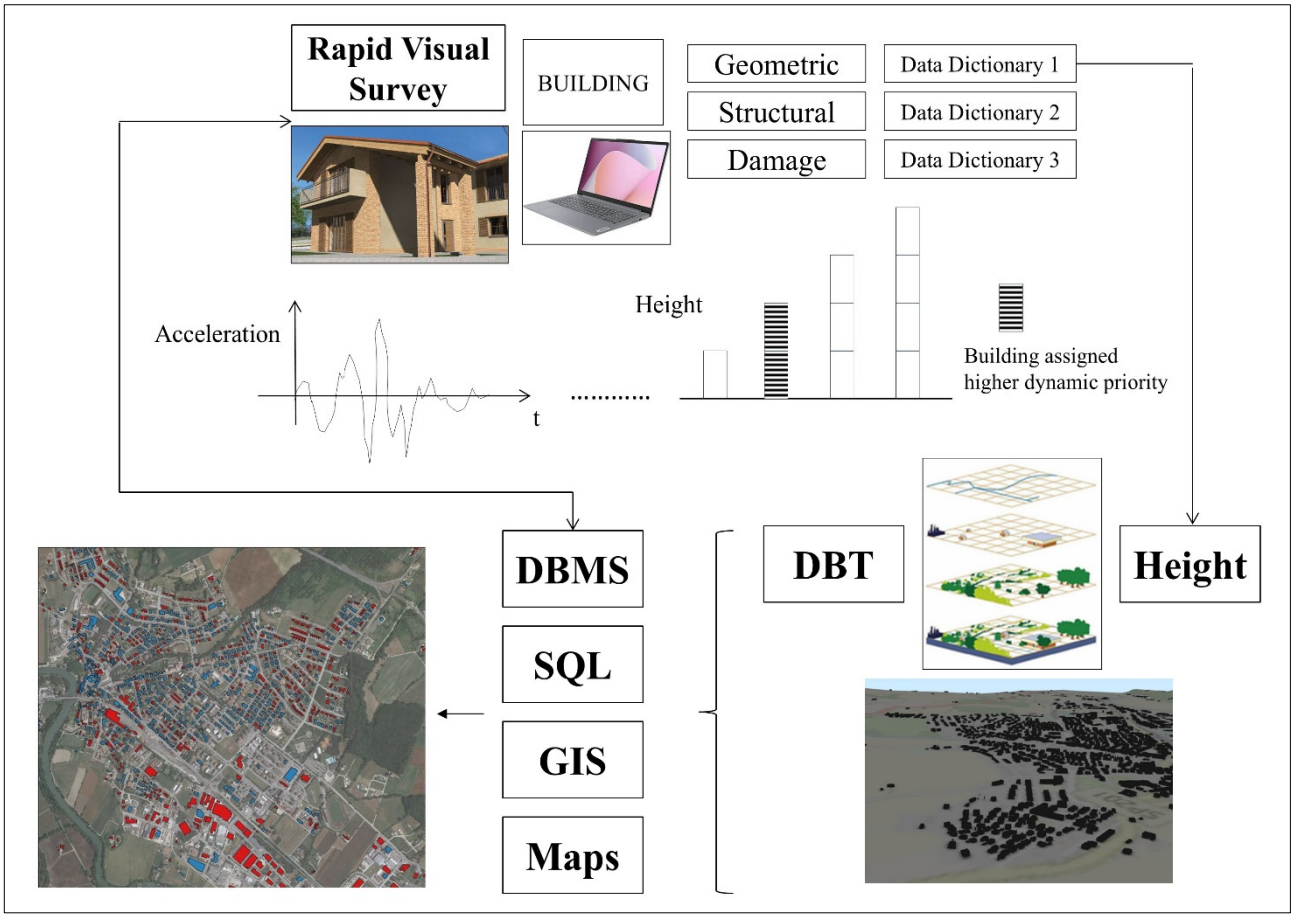


Figure 1. Three-phase workflow of the proposed method: rapid visual survey and data structuring; processing of recorded ground accelerations to identify building-height classes with higher dynamic priority; and integration of DBMS, DBT, SQL, and GIS for mapping the selected buildings.

2.2. Data Structuring

The data acquired during the rapid survey constitute the core of the geometric-structural information on the building and were defined by taking into account the indications provided by the National Technical Regulations [1].

In the proposed method, building height, or the number of storeys above ground, represents the parameter directly related to the spectral amplification ratio derived from the recorded ground motion.

The other data collected during the rapid visual survey do not all enter the DAF calculation, but are necessary to build a queryable urban inventory, select masonry buildings, characterize their use, construction period, materials, observable conditions and possible

damage, and support subsequent verification or detailed analysis phases. In this way, the height-based spectral indicator is included within a broader information structure, which can be used in the DBMS and GIS for queries, filters, and cartographic representations.

The information is organized in the BUILDING table. Some of its fields are associated with data dictionaries, which can be selected during the survey through drop-down menus, in order to make data entry faster and, at the same time, to ensure more homogeneous subsequent database queries. The complete list of BUILDING-table fields and the corresponding data dictionaries is provided in Appendix A.

The fields of the BUILDING table are shown in Figure 2 together with the corresponding dictionaries.

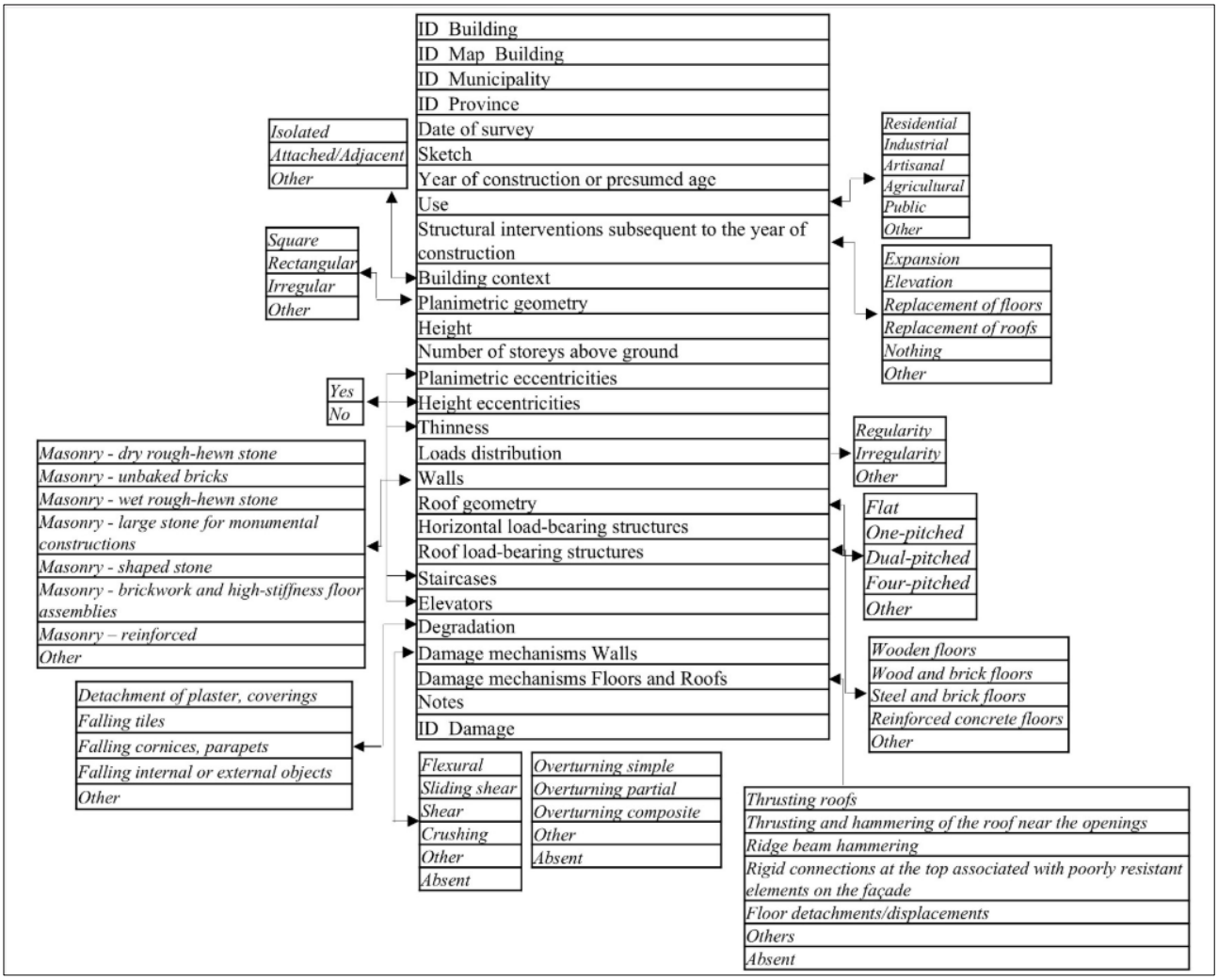


Figure 2. Building table fields along with their corresponding dictionaries (in italics).

The database also includes information relating to the accelerometric recording stations, the authorities managing the seismic networks, the earthquakes acquired from their institutional archives, the results of the accelerometric processing, and the earthquake damage recorded during the survey.

The STATION table consists of alphanumeric information from the seismic network stations (National Seismic Network RSN and National Accelerometric Network RAN) that record the ground accelerations. The ADMINISTRATION table consists of alphanumeric information on the authorities that install and manage the seismic networks (for example

DPC or INGV). The EARTHQUAKE table consists of alphanumeric information relating to the earthquake.

The PERIOD AMPLITUDE DAF HEIGHT/STOREY table contains alphanumeric information relating to the oscillator period T, peak ground acceleration (PGA), the spectral amplification ratio DAF(T) = A(T)/PGA, and the corresponding critical height Hc or equivalent number of critical storeys Pc derived from the accelerometric recordings processed as described in Section 2.3.

The DAMAGE table consists of alphanumeric information relating to earthquake-induced damage to the buildings according to a previously defined scale of values. The records reported in Table 1 correspond to this table.

Table 1. Numerical damage scale.

ID_Damage	Type	Value	Full Description
1	Absent	0	No damage
2	Low	1	Small number of light superficial fissures in the plaster a few millimetres wide. Horizontal displacements without expulsion of material
3		2	Diffuse light superficial fissures. Limited separations. Falls of small pieces of plaster or stucco not bound to the wall and degraded
4	Medium	3	Superficial fissures and some deep fissures 1 cm wide. Damage to the roof. Possible falls of non-structural objects
5		4	Numerous superficial fissures and deep fissures 1 cm wide or wider near the openings (crushing mechanism). Slight separations between floor assemblies and/or staircases and orthogonal walls (of 1 mm). Lesions to the vaults of several millimetres and/or with symptoms of crushing
6		5	Numerous superficial fissures and deep fissures 1 cm wide distributed on parts of the building. Detachments in the secondary framework of the floor assemblies and displacements of up to 1 cm of the main beam supports. Significant damage to the roof with falls of tiles. Visible non-verticalities
7	High	6	Structural damage compromising the safety of the residents. Parts of the structure damaged but not in imminent danger
8		7	Structural damage causing instability. Parts of the structure damaged and separated from the body of the building. Significant separations between floor assemblies and/or staircases and walls and between orthogonal walls of ca. 1 cm
9		8	Structural damage compromising stability. Parts of the structure detached by building collapse and partial collapses. Non-verticality with lesions passing through the masonry
10	Very high	9	Diffuse structural collapses, but most of the structure still recognizable with danger risk for the residents (instability-dangerousness). Collapse of 50% of the building
11		10	Complete or almost complete collapse

The STATION EARTHQUAKE table is the many-to-many connection table between the STATION table and the EARTHQUAKE table. The BUILDING EARTHQUAKE table is the many-to-many connection table between the BUILDING table and the EARTHQUAKE table.

The complete lists of fields included in the STATION, ADMINISTRATION, EARTHQUAKE, PERIOD AMPLITUDE DAF HEIGHT/STOREY, DAMAGE, STATION EARTHQUAKE, and BUILDING EARTHQUAKE tables are provided in Appendix A.

Figure 3 represents the type of structuring, constituting a DBMS entity-relationship model (or ER model; [87–89]) in which the relationships are indicated by arrows placed in correspondence to the key fields (highlighted in italics).

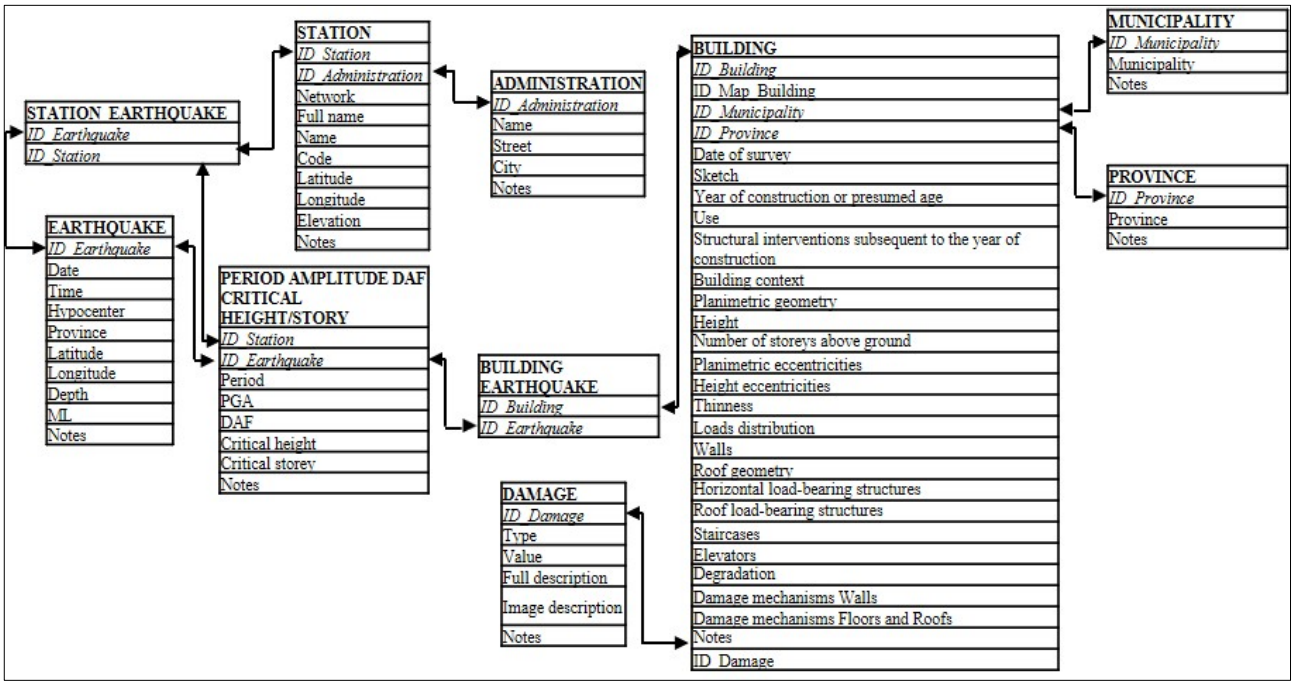


Figure 3. Entity-relationship model (or ER model) of the DBMS.

2.3. Accelerometric Processing Procedure

The relationship between building height and the spectral amplification ratio (DAF) is established by processing the ground-acceleration records acquired by the seismic stations during an earthquake. From these records, pseudo-acceleration spectra are derived, and the DAF is first calculated as a function of the spectral period T and then related, through the empirical period-height relationship, to building height or number of storeys above ground. Figure 4 shows a simplified flow chart of the accelerometric data processing.

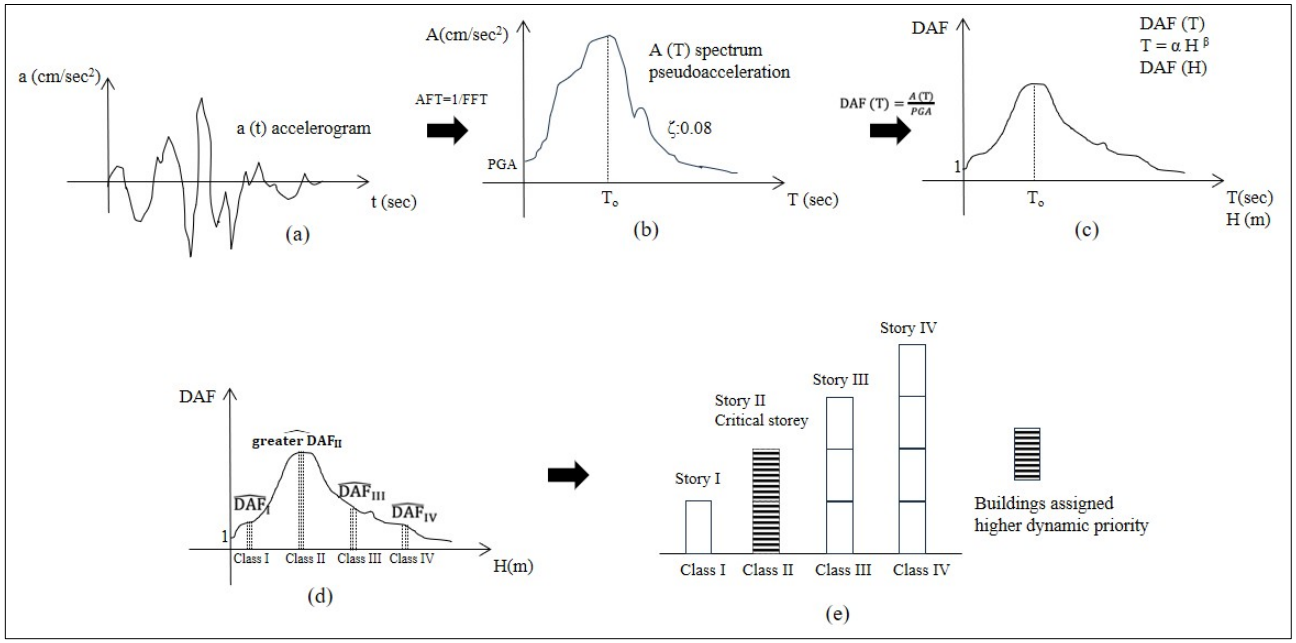


Figure 4. Simplified flow chart of the accelerometric data processing: (**a**) ground-acceleration record; (**b**) pseudo-acceleration spectrum; (**c**) calculation of DAF(T) and conversion to DAF(H); (**d**) comparison of the class-mean DAF values; and (**e**) identification of the critical storey class and assignment of higher dynamic priority.

The ground-acceleration records, acquired along the North/South and East/West directions (Figure 4a), were first converted to cm/s^2, subjected to a linear baseline correction, and filtered in the time domain using a second-order Butterworth band-pass filter, with lower and upper cut-off frequencies of 0.1 and 50 Hz, respectively [90–92].

The filtered horizontal records were subsequently processed using MATLAB R2025a (MathWorks, Natick, MA, USA) [93] to calculate the displacement, velocity, and pseudo-acceleration response spectra through an IFFT-based procedure. The spectra were computed over the period range T = 0–0.6 s, with an increment dT = 0.002 s and a damping ratio of 8%, as suggested for masonry buildings by Jeary [94], ESDU [95], Chopra [96], Fang et al. [97], Satake et al. [98], Lin et al. [99], Elnashai and Di Sarno [100], and Gatti [101].

In the adopted spectral procedure, the damping ratio affects the spectral ordinates and the amplitude of the spectral maximum, but not the period T_0 at which that maximum occurs; therefore, it does not alter the corresponding height or the identified critical storey P_c.

The mean pseudo-acceleration spectrum was obtained as the arithmetic mean of the spectral ordinates of the two horizontal components (Figure 4b).

From the mean spectrum, the spectral amplification ratio DAF(T) is calculated over the previously specified period range and increment using Formula (1), where A(T) is the ordinate of the mean pseudo-acceleration spectrum and PGA is the mean peak ground acceleration of the two horizontal components, corresponding to the spectral ordinate at T = 0 (Figure 4c).

$$\mathrm{DAF(T)} = \frac{A(\mathrm{T})}{PGA} \tag{1}$$

The physical basis of this conversion is a conservative period-matching assumption. The recorded ground motion is represented through its pseudo-acceleration response spectrum, which expresses the maximum response of an equivalent single-degree-of-freedom oscillator as a function of its natural period T. For screening purposes, each masonry building is likewise idealized as an equivalent oscillator, whose estimated fundamental period is matched to the corresponding spectral period. Within this simplified representation, period coincidence corresponds to the most unfavourable resonance-type condition, while the highest DAF values identify the period ranges associated with the largest dynamic demand. The empirical period-height relationship is therefore used to associate each spectral period with the corresponding building height and number of storeys. To convert the spectral period T into the corresponding building height, the inverse of the following code-based empirical period-height relationship, widely adopted in seismic design for the simplified estimation of the fundamental period, is used:

$$\mathrm{T} = \alpha\, \mathrm{H}^{\beta} \tag{2}$$

where H is expressed in metres. For masonry buildings, the coefficients $\alpha = 0.05$ and $\beta = 0.75$ are adopted in accordance with ATC [102], Goel and Chopra [103], SEAOC [104], Hong and Hwang [105], and CEN [106].

These coefficients were adopted directly from the code-based empirical period–height relationship for masonry buildings and were not calibrated against either the investigated building stock or the observed damage. Their use preserves a standardised and replicable screening procedure.

Over the complete spectral range T = 0–0.6 s, the inverse of Equation (2) corresponds to building heights ranging from 0 to approximately 27.47 m. However, the present screening analysis is restricted to the four masonry-building height classes defined below, extending up to approximately 12.5 m, which corresponds to $T \approx 0.33$ s.

At the end of the procedure, an equivalent DAF curve is obtained, with building height H replacing spectral period T on the x-axis (Figure 4c).

Discrete representative heights were adopted rather than continuous height intervals because the Italian building stock is characterised by recurrent standard storey heights associated with different construction periods and building practices [107]. Accordingly, four classes were defined, from I to IV, each represented by a triplet of total building heights derived from these recurring standards: 2.70, 2.85, and 3.00 m for Class I; 5.50, 5.75, and 6.00 m for Class II; 8.50, 8.75, and 9.00 m for Class III; and 11.50, 11.75, and 12.00 m for Class IV. These classes correspond, respectively, to one, two, three, and four storeys above ground. The use of three discrete heights within each class allows the class-mean DAF to be evaluated without assuming a continuous distribution of building heights.

For each height value H belonging to a given class, the corresponding spectral amplification ratio $DAF_i(H_i)$ is calculated; the mean value for the three heights of the class is then obtained:

$$\widehat{DAF_{C_J}} = \sum_{i=1}^{3} \frac{DAF_{i(H_i)}}{3} \quad (3)$$

In Formula (3), J varies from I to IV.

The highest of the four class-mean values identifies the height class, and therefore the number of storeys above ground, associated with the highest spectral amplification ratio derived from the recorded ground motion (Figure 4d). This number of storeys is defined as the critical storey Pc. Buildings with a number of storeys equal to Pc are not considered vulnerable in absolute terms; rather, they are assigned a higher dynamic priority for subsequent inspections or detailed analyses (Figure 4e).

2.4. Cartographic Database

The cartographic database used first for the survey and then to extract the maps was imported from a regional numerical database created from direct survey sources, such as terrestrial, aerial photogrammetric and satellite surveys. Its elements consist of buildings, streets, house numbering, water bodies, etc., according to three file types in the ESRI standard:

- A file with .shp extension (shape file) containing the coordinates of the vertices of the polygons, lines or points of the above-mentioned elements;
- A file with .dbf extension in which their attributes are stored;
- A file with .shx extension which acts as an index between the attributes and the coordinates.

The cartographic database was associated with the information relating to the number of storeys above ground recorded during the survey. In this way, the two-dimensional cartography of the building stock was integrated with the height data and used as a three-dimensional database for the subsequent GIS queries and map representations. To take into account the topography of the ground, a digital terrain model (DTM), created from data acquired from the LiDAR platform, was added to the cartographic database.

3. Case Study

The method was tested in an area including the municipalities of Umbertide and Gubbio, in the province of Perugia, central Italy, affected by the earthquake of 9 March 2023. The seismic sequence consisted of three main events: UTC 15:05:40, Ml = 4.4; UTC 19:08:04, Ml = 4.6; and UTC 19:13:56, Ml = 3.9. The epicentres, located about 6 km from Umbertide, were distributed a few hundred metres from each other (Figure 5).

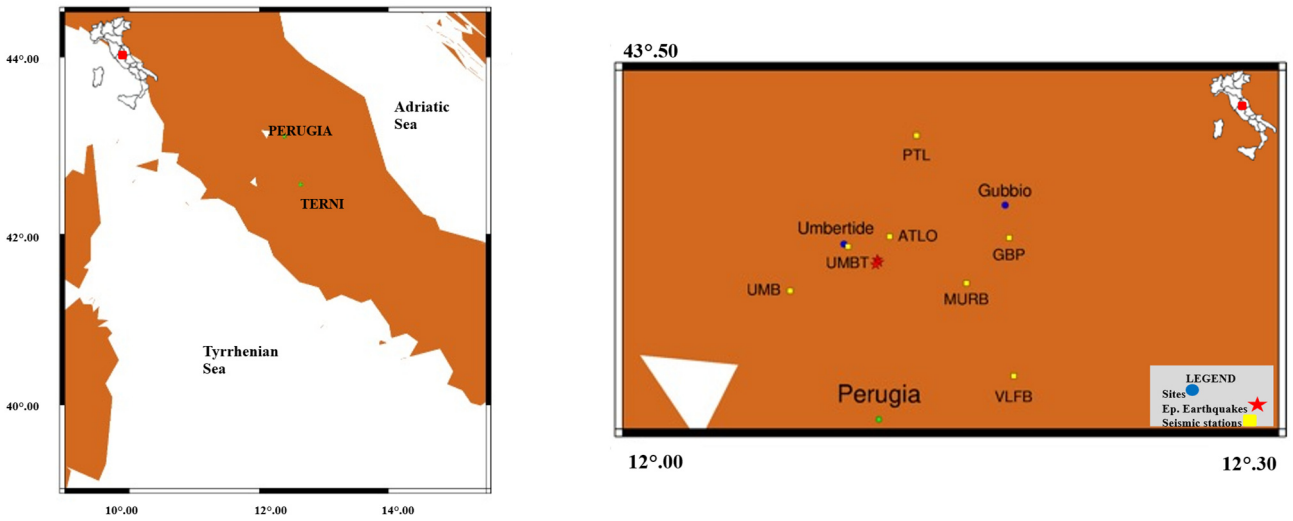


Figure 5. Study area, earthquake epicentres and seismic stations.

3.1. Rapid Visual Survey

After the earthquake, in spring 2023, two teams used handheld PDAs equipped with the cartographic database of the Umbria Region [108], pre-compiled digital tables with drop-down menus, and built-in photographic devices. The teams surveyed an average of 300 buildings/day, recording geometric and structural data and assigning the corresponding number of storeys above ground to each building.

During the survey, the buildings damaged by the 9 March 2023 earthquake were also identified, and the damage value described in Table 1 was assigned to each of them. In about fifteen days of field activity, around 7000 masonry buildings were recorded in Gubbio and just over 4000 in Umbertide, including those damaged by the earthquake of 9 March 2023, the latter representing a very low percentage, less than 1%.

3.2. Accelerometric Data Processing

The study area included the accelerometric recording stations of Gubbio Piana (GBP), Umbertide (UMB and UMBT), Monte Urbino (MURB), Valfabbrica (VLFB), Montelovesco (ATLO) and Pietralunga (PTL), belonging to both the National Seismic Network (RSN) of the National Institute of Geophysics and Volcanology (INGV) and the National Accelerometric Network (RAN) of the Department of Civil Protection (Figure 5). All the available accelerometric records from the stations listed above were processed individually. The method deliberately exploits the permanent seismic networks already operating in the territory, whose continuous monitoring provides ground-motion records of the actual seismic event without requiring dedicated instrumentation campaigns. With respect to the reference coordinates adopted for the two investigated localities, the stations were located at geodetic distances ranging from approximately 2.2 to 28.2 km from Umbertide and from approximately 5.2 to 29.0 km from Gubbio. The nearest stations were UMBT for Umbertide and GBP for Gubbio, whereas the farthest were VLFB and UMB, respectively. These distances are reported solely to describe the spatial distribution of the available recording stations. They were not used to assign individual buildings to specific stations or to apply quantitative spatial weights to the results.

These stations were equipped with triaxial accelerometers, in the North/South, East/West and $\pm$Z (up) directions, and recorded the above-mentioned seismic events with a sampling frequency of 200 Hz.

The results of the data processing carried out following the procedure described in Section 2.3 were summarized in Tables 2 and 3 for each recording station and for each of the

three events of the 9 March earthquake. Table 2 reports the distance d_e (km) of the station from the epicentre, the peak ground acceleration (PGA (g)), the mean significant duration t_d (s) of the earthquake [109–111], the period T_0 (s) corresponding to the maximum ordinate of the mean pseudo-acceleration spectrum and the maximum spectral amplification ratio DAFmax. The pseudo-acceleration spectral ordinates were calculated using a damping ratio of 8%, as assumed for masonry buildings.

Table 2. Earthquakes, seismic stations, and DAF_{max} for a damping ratio equal to 8%.

Earthquake	Seismic Station	d_e (km)	PGA (g)	t_d (s)	T_0 (s)	DAF_{max}
UTC 15:05:40 Ml 4.4	ATLO	3.3	0.08	3	0.044	2.6
	UMBT	3.8	0.13	8	0.200	2.4
	MURB	11.4	0.07	6	0.212	2.6
	UMB	11.8	0.05	5	0.070	2.4
	PTL	15.3	0.04	5	0.122	2.8
	GBP	16.3	0.13	6	0.198	2.7
UTC 19:08:04 Ml 4.6	ATLO	3.5	0.08	4	0.060	3
	UMBT	4.2	0.04	13	0.166	2.9
	MURB	11.2	0.12	5	0.256	3.6
	UMB	11.3	0.03	7	0.064	3.2
	GBP	16.5	0.08	9	0.208	2.8
	VLFB	21.9	0.09	3	0.126	3.1
UTC 19:13:56 Ml 3.9	ATLO	3.9	0.05	2	0.056	2.8
	MURB	11.5	0.03	5	0.168	3.0
	GBP	16.9	0.05	4	0.194	3.7

Table 3. Earthquakes, seismic stations, maximum mean DAF, critical height H_c and critical storey P_c.

Earthquake	Seismic Station	Maximum Mean DAF	Class	H_c (m)	P_c
UTC 15:05:40 Ml 4.4	ATLO	1.6	I	2.7–2.85–3.0	1
	UMBT	2.3	II	5.5–5.75–6.0	2
	MURB	2.4	II	5.5–5.75–6.0	2
	UMB	2	III	8.5–8.75–9.0	3
	PTL	2.5	III	8.5–8.75–9.0	3
	GBP	2.5	II	5.5–5.75–6.0	2
UTC 19:08:04 Ml 4.6	ATLO	1.7	I	2.7–2.85–3.0	1
	UMBT	2.7	II	5.5–5.75–6.0	2
	MURB	3.6	III	8.5–8.75–9.0	3
	UMB	1.8	I	2.7–2.85–3.0	1
	GBP	2.7	II	5.5–5.75–6.0	2
	VLFB	3.0	III	8.5–8.75–9.0	3
UTC 19:13:56 Ml 3.9	ATLO	1.4	I	2.7–2.85–3.0	1
	MURB	2.5	II	5.5–5.75–6.0	2
	GBP	3.5	II	5.5–5.75–6.0	2

Table 3 reports the highest mean spectral amplification ratio calculated according to Equation (3), together with the corresponding building class, trio of heights, and critical storey P_c, as derived from the ground-acceleration records acquired by the seismic stations.

Table 2 shows that, during the earthquakes of 19:08:04 ML 4.6 and 19:13:56 ML 3.9, the seismic stations of Montelovesco, Monte Urbino, Valfabbrica and Gubbio Piana, close to the municipalities of Umbertide and Gubbio, recorded PGA values varying from a minimum of 0.03 g up to a maximum of 0.13 g, with maximum spectral amplification ratios reaching and, in some cases, exceeding 3, although characterized by seismic sequences of low mean significant duration.

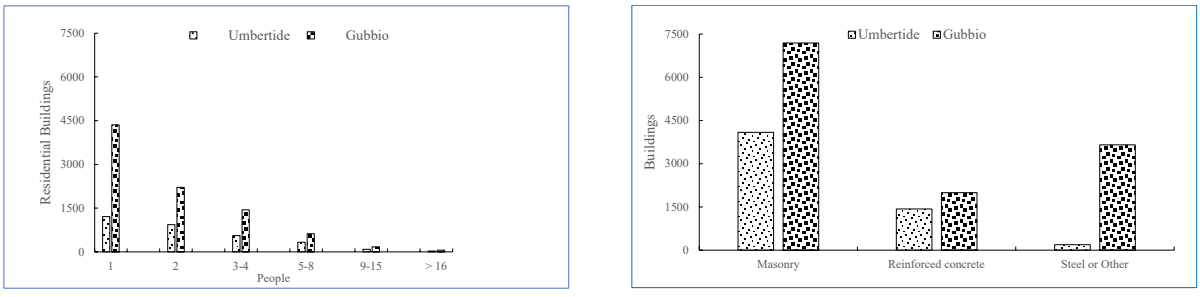
Table 3 shows that the critical classes identified by the model comprised Classes I, II and III, corresponding to one-, two- and three-storey masonry buildings. Class I was identified in four of the fifteen processed records, Class II in seven records, and Class III in four records. For the illustrative application of the GIS extraction and mapping procedure, the case study focused on Classes II and III. This choice does not exclude Class I from the model results; it limits the cartographic representation to the two- and three-storey classes in order to demonstrate the operational GIS procedure.

3.3. DBMS and GIS

Both the data from the rapid survey and those obtained from the processing of the accelerometric measurements were entered into the DBMS in order to perform the subsequent queries. The queries did not concern only building height or the number of storeys above ground, used for the dynamic correlation, but also the other attributes collected during the survey, which were necessary to select masonry buildings, distinguish them by use, material and construction period, and compare the identified classes with the observed damage. The results of the queries were organized and represented in the GIS and are described in the following sections.

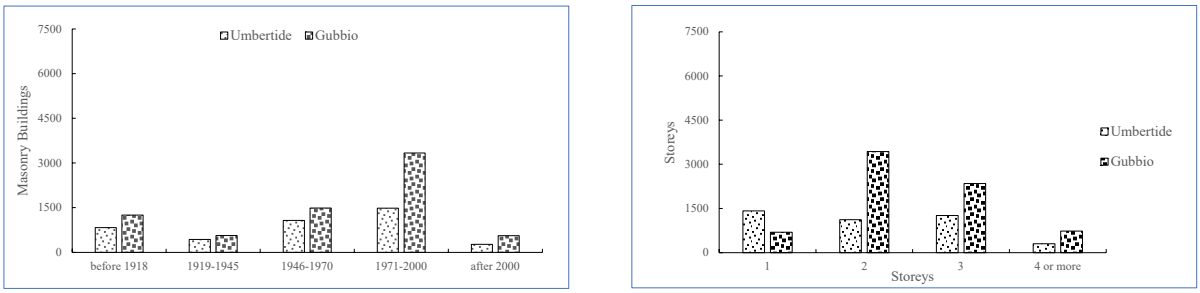
3.3.1. Buildings

Fewer than 6000 buildings were recorded in the municipality of Umbertide and approximately 13,000 in that of Gubbio. Of these, respectively, just over 3000 and less than 9000 were used as residences, mainly occupied by one- and two-member households (Figure 6a). Figure 6b shows the number of residential and non-residential buildings by construction material: masonry buildings accounted for just over 4000 in Umbertide and just over 7000 in Gubbio. They were mostly constructed after 1970, although with a non-negligible number of buildings dating to before 1918: approximately 850 in Umbertide and 1300 in Gubbio (Figure 7a). In Figure 7b, the same buildings are shown according to the number of storeys above ground, from which it can be observed that the prevailing masonry typology consists of two- and three-storey buildings.



(**a**) (**b**)

Figure 6. Masonry buildings. (**a**) Residential buildings and number of occupants. (**b**) Number of buildings by construction material.



(**a**) (**b**)

Figure 7. Masonry buildings. (**a**) Construction period. (**b**) Number of storeys above ground.

As shown in the previous figures, masonry buildings represented 55% of the total in Umbertide and 69% in Gubbio. Among them, two- and three-storey buildings accounted for 58% in Umbertide and 80% in Gubbio; moreover, 45% in Umbertide and 38% in Gubbio were built between the post-war period and the end of the twentieth century, that is, before the full application of modern Italian anti-seismic design standards.

3.3.2. Preliminary Seismic-Risk Prioritization Related to Building Height

For the illustrative GIS application described above, the queries were extended from the DBMS to the GIS and restricted to masonry buildings belonging to Classes II and III. In the municipality of Umbertide, with an area of 200 km^2 and a mean density of 28 buildings/km^2, approximately 1116 two-storey buildings and 1256 three-storey buildings were selected, corresponding to 2372 of the 4089 masonry buildings. A 1:10,000-scale map extracted from the historic centre of Umbertide illustrates, within an area of a few square kilometres, the high density of two-storey buildings, in red, and three-storey buildings, in blue (Figure 8).

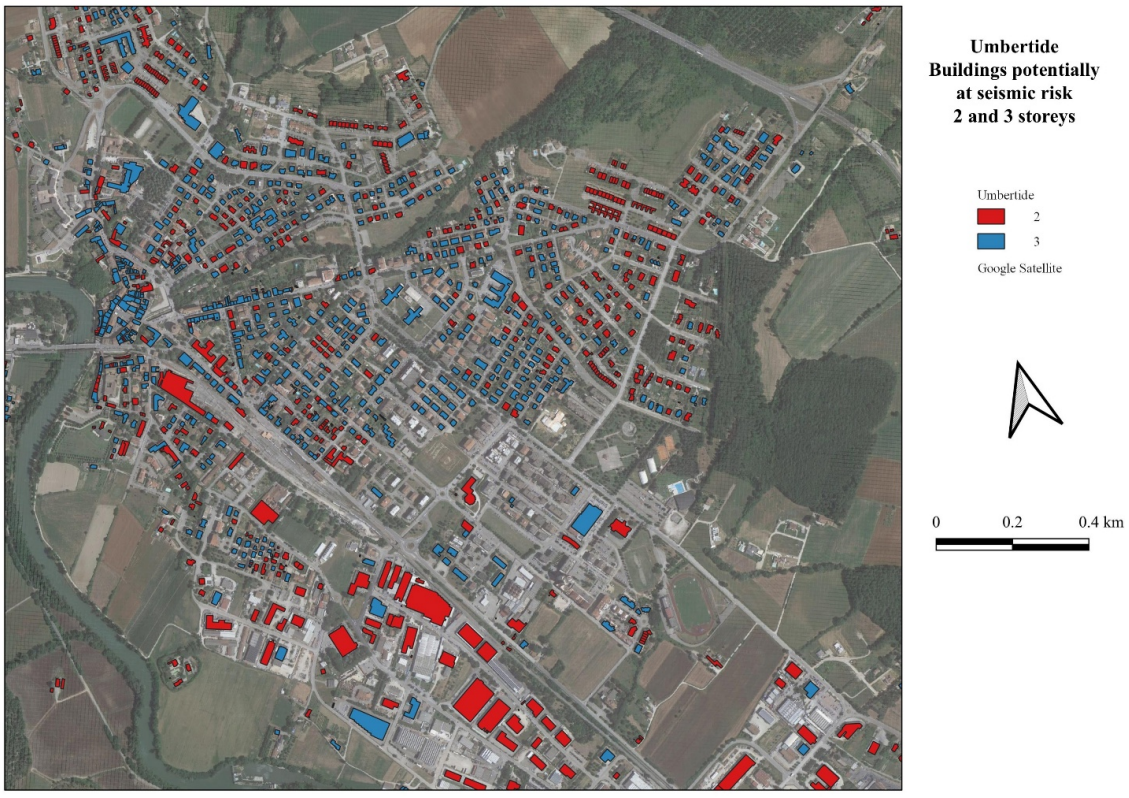


Figure 8. Illustrative GIS map of two- and three-storey masonry buildings in an area of the historic centre of Umbertide.

The municipality of Gubbio has a larger area, equal to 525 km^2, but a lower mean density of 24 buildings/km^2. The same illustrative GIS extraction selected approximately 3431 two-storey buildings, in red, and approximately 2342 three-storey buildings, in blue, corresponding to 5773 of the 7192 masonry buildings. Their distribution is shown in a 1:10,000-scale map covering a larger area of the historic centre of Gubbio (Figure 9).

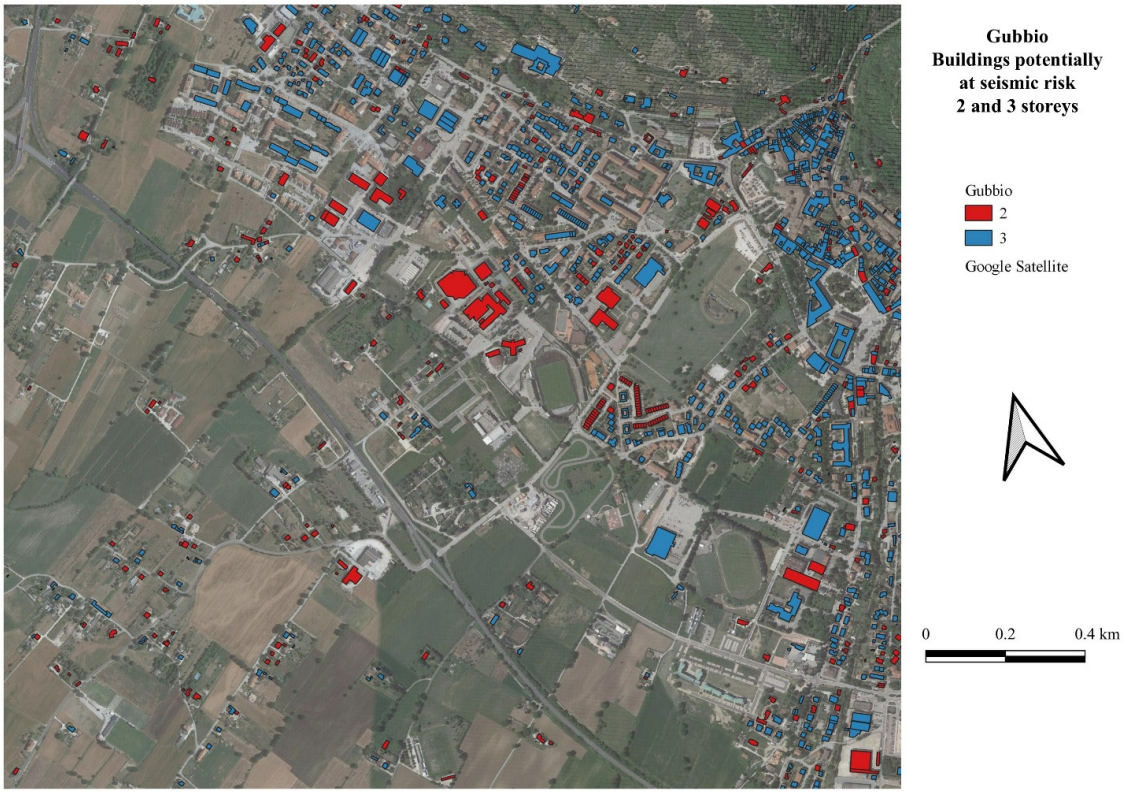


Figure 9. Illustrative GIS map of two- and three-storey masonry buildings in an area of the historic centre of Gubbio.

3.4. Verification of the Method

In the operational phase, the model first identifies the critical number of storeys from each processed accelerometric record. The GIS can then be queried to select and map masonry buildings belonging to any of the identified storey classes. In the present case study, the cartographic application was limited, for illustrative purposes, to Classes II and III. Observed damage was not used as an input to the model or as a criterion for this GIS extraction. The post-earthquake damage survey was used only for a subsequent preliminary verification, by assessing the correspondence between the cartographically represented classes and the distribution of the observed damage, without excluding the Class I results identified by the model.

The damaged buildings recorded during the survey were located in Pierantonio, Umbertide centre, and Montecorona, within the municipality of Umbertide; in Gubbio; and in Sant'Orfeto–La Cinella, within the municipality of Perugia. For the preliminary numerical comparison, the sample was restricted to 33 masonry buildings, including one confined-masonry building; three reinforced-concrete buildings recorded during the same survey were excluded. Of the 33 buildings, 17 were located in Pierantonio, four in Umbertide centre, four in Montecorona, seven in Gubbio, and one in Sant'Orfeto–La Cinella. Approximately 45% of the sample was built between 1945 and 1990, while 55% pre-dated 1945. The main wall typologies were masonry walls (55%) and irregular-stone masonry, alone or combined with masonry walls (39%); confined masonry and brick masonry each

accounted for 3%. The floor assemblies were mainly made of brick and reinforced concrete (52%), followed by wood (21%), steel and brick (15%), and wood and brick (6%); floor data were unavailable for the remaining 6%. The roofs were mainly made of brick and reinforced concrete (48%), wood (33%), steel and brick (12%), and wood and brick (6%). Residential use accounted for 82% of the sample, while public and artisanal uses accounted for 15% and 3%, respectively. Attached or adjacent buildings represented 58% of the sample, while 42% were isolated. In-plane wall damage mechanisms were recorded in 32 buildings, while out-of-plane mechanisms were recorded in eight buildings, with some buildings exhibiting both types. Mechanisms involving floor or roof structures and interactions between adjacent buildings were each recorded in only one case. Figure 10 shows the damaged buildings located in Pierantonio (a), Sant'Orfeto–La Cinella (b), Umbertide centre (c), and Gubbio (d), according to the damage values defined in Table 1 and represented by shades of blue. The buildings recorded in Montecorona are included in the numerical comparison. The maps include all the damaged buildings recorded during the survey, whereas the subsequent numerical comparison excludes the three reinforced-concrete buildings.

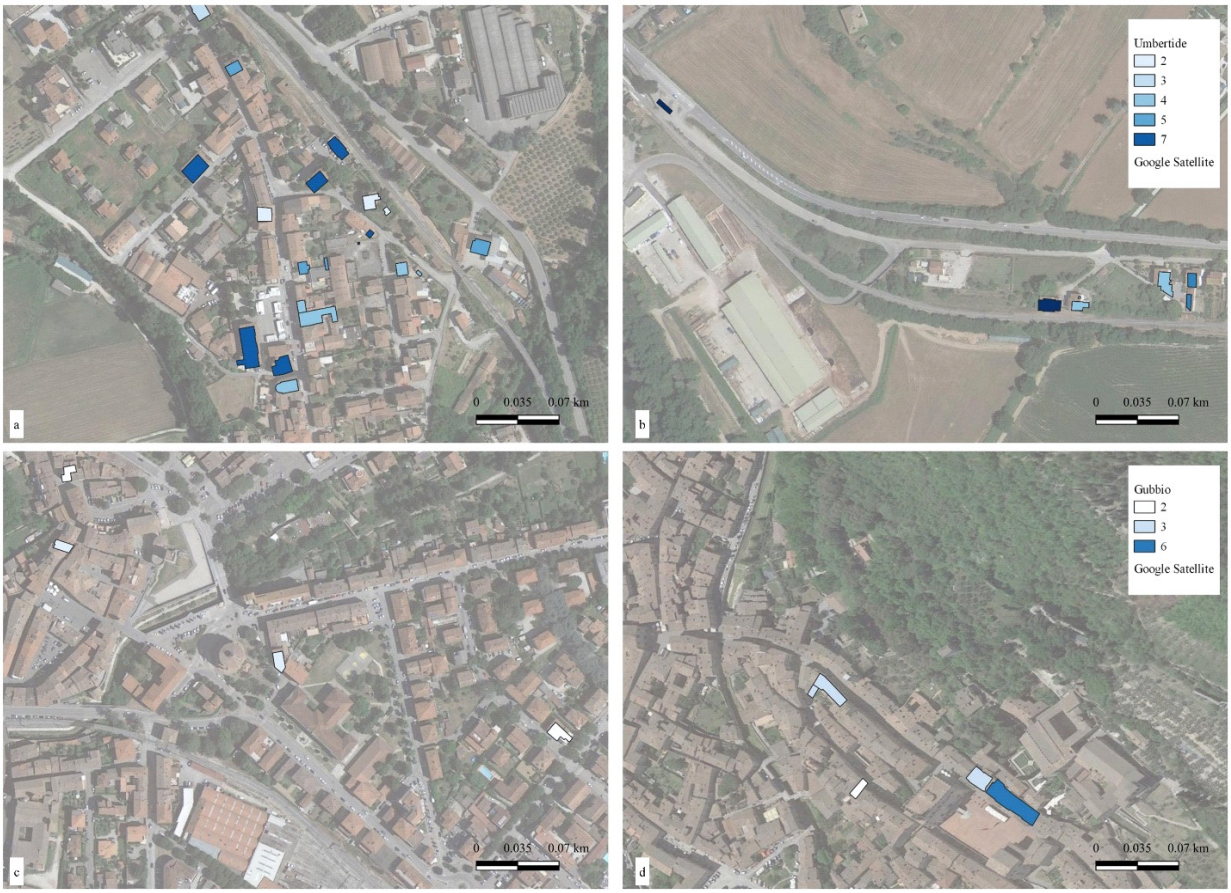


Figure 10. Maps of damaged buildings with damage levels represented by shades of blue: (**a**) Pierantonio; (**b**) Sant'Orfeto–La Cinella; (**c**) Umbertide centre; (**d**) Gubbio.

The damage values ranged from 1 to 9, with a mean value of 4.5 ± 2.1. One two-storey building located in Montecorona had very high damage, corresponding to a value of 9. High damage values, ranging from 6 to 8, were recorded in ten buildings.

Table 4 reports the number and percentage of the 33 masonry buildings included in the preliminary comparison, classified according to damage level and number of storeys. Percentages are calculated with respect to the total sample.

Table 4. Distribution of the 33 masonry buildings included in the preliminary comparison by damage level and number of storeys; values are expressed as *n* (% of the total sample).

Damage/Storey	1	2	3	4	5
Low (from 1 to 2)	0 (0%)	1 (3%)	2 (6%)	4 (12%)	0 (0%)
Medium (from 3 to 5)	2 (6%)	2 (6%)	11 (33%)	0 (0%)	0 (0%)
High (from 6 to 8)	0 (0%)	4 (12%)	6 (18%)	0 (0%)	0 (0%)
Very high (from 9 to 10)	0 (0%)	1 (3%)	0 (0%)	0 (0%)	0 (0%)

As shown in Table 4, 22 of the 33 buildings (67%) had damage values of 5 or less, corresponding to low or medium damage. The largest single group consisted of 11 three-storey buildings with medium damage, accounting for 33% of the sample. Damage values of 6 or more, corresponding to high or very high damage, were recorded in 11 buildings (33%): five two-storey buildings (15%) and six three-storey buildings (18%). Overall, two- and three-storey buildings accounted for 27 of the 33 masonry buildings included in the comparison (82%). The mean number of storeys above ground was 2.8 ± 0.8. These percentages describe the distribution within the damaged-building sample and are not normalised by the total number of buildings belonging to each storey class.

Class-specific damage ratios could not be estimated because the post-earthquake damage survey was not exhaustive and the damaged-building sample was not spatially coextensive with the municipal building inventories. In particular, it included buildings from different localities and one building located outside the municipalities of Umbertide and Gubbio. The available municipal totals therefore do not provide homogeneous denominators for calculating reliable damage incidence ratios by storey class.

The comparison therefore indicates a preliminary application-based correspondence between the cartographically represented classes and the observed damage distribution, without excluding the Class I results identified by the model.

3.5. Discussion and Comparison with RVS Approaches and the Literature

The results obtained in the case study make it possible to compare the classes identified by the dynamic screening with the distribution of the damage observed after the earthquake of 9 March 2023.

The comparison reported in Table 5 distinguishes between the classes identified by the dynamic screening and those selected for the illustrative GIS application. The processed accelerometric records identified Classes I, II and III, whereas the cartographic representation focused on Classes II and III. These two classes comprised 27 of the 33 masonry buildings included in the damaged-building sample (82%), whose mean number of storeys was 2.8 ± 0.8. As noted above, this percentage is not normalised by the total number of buildings belonging to each storey class. The comparison therefore indicates a preliminary application-based correspondence between the cartographically represented classes and the observed damage distribution, without excluding the Class I results produced by the model.

Table 5. Preliminary application-based comparison between the illustrative GIS extraction and the observed damage in the case study.

Element of Comparison	Result Obtained	Interpretation
Classes identified by the dynamic screening	Classes I, II and III	One-, two-, and three-storey masonry buildings identified from the processed accelerometric records
Critical storeys (P_c)	1–3 storeys above ground	Storey classes associated with the highest class-mean spectral amplification ratios for the individual records

Table 5. *Cont.*

Element of Comparison	Result Obtained	Interpretation
Buildings selected in the illustrative GIS extraction—Umbertide	2372 buildings out of 4089	Illustrative selection of the two- and three-storey masonry buildings
Buildings selected in the illustrative GIS extraction—Gubbio	5773 buildings out of 7192	Illustrative selection of the two- and three-storey masonry buildings
Mean number of storeys of damaged buildings	2.8 ± 0.8	Consistency with Classes II and III selected for the illustrative GIS mapping
Buildings with high or very high damage	11 buildings: 5 two-storey and 6 three-storey	Distribution within the damaged-building sample; not normalised by the total number of buildings in each storey class
Type of verification	Preliminary and application-based	The comparison does not exhaust seismic vulnerability, but supports the use of the method for prioritization

Table 6 provides a summary of the data used, the results produced, the advantages and limitations of the approaches reported in the literature, as well as a comparison with the proposed method.

Table 6. Comparison between the proposed method and selected rapid, RVS, GIS-based and predictive approaches reported in the literature.

Approach	Main Data Used	Result Produced	Advantages	Limitations	Comparison with the Proposed Method
Traditional RVS approaches, FEMA P-154/P-155	Visual observation, structural typology, irregularities, height, use, construction age	Preliminary vulnerability/priority score or class	Established, rapid and standardized method	Depends on the survey form and on the surveyor's experience; does not directly integrate local accelerometric recordings	The proposed method is complementary: it does not replace the RVS form, but adds a dynamic level based on DAF and height
Risk-UE or LM2-type approaches	Typological classes, vulnerability of the building stock, territorial scenarios	Vulnerability estimate or damage scenario at urban/territorial scale	Suitable for territorial assessments and risk scenarios	Require typological classifications and multiple parameters that are not always available in a rapid phase	The proposed method is more circumscribed and operational, useful for a first selection of buildings to be investigated further
GIS-based approaches	Territorial databases, cartography, building attributes, exposure or vulnerability indicators	Thematic maps of vulnerability, exposure or risk	Strong capacity for spatial representation and data querying	The local dynamic component may be absent or treated indirectly	The proposed method integrates GIS and DBMS with local accelerometric data
Soft computing/machine learning approaches	Structured datasets, building parameters, observed damage, predictive models	Damage/vulnerability classifications or predictions	High predictive capacity when the data are extensive and reliable	Require extensive datasets, training and validation	The proposed method requires fewer data and can be applied rapidly after an event
Proposed method	Rapid survey, height/number of storeys, DBMS, GIS, accelerograms, DAF	Preliminary prioritization of masonry buildings	Rapid, replicable, integrates local geometric and dynamic data, and produces operational maps	Does not provide a global vulnerability assessment; mainly considers the height parameter in relation to the dynamic response and requires local accelerometric recordings	Decision-support tool to be used alongside complete RVS procedures, post-event inspections, and subsequent structural analyses

The rows distinguish five main categories: traditional RVS approaches, represented in particular by FEMA P-154/P-155; typological-vulnerability approaches, such as Risk-UE or LM2; GIS-based approaches; approaches based on soft computing and machine learning; and, finally, the proposed method.

The comparison shows that traditional RVS approaches and typological-vulnerability approaches respectively produce preliminary vulnerability scores or damage scenarios, but do not directly integrate local accelerometric recordings into the selection of buildings. GIS-based approaches provide a strong capacity for data management and spatial representation, but the local dynamic component may remain absent or be treated indirectly. Soft computing and machine learning approaches have high predictive capacity, but require extensive datasets, training and validation.

In this framework, the proposed method should be regarded as an integrative and operational screening tool. It combines rapid geometric information, DBMS/GIS management and local accelerometric data to support a first spatial prioritization of masonry buildings, without replacing complete seismic vulnerability assessment procedures.

Unlike conventional RVS methods, which derive priority mainly from observed building characteristics or typological vulnerability classes, the proposed workflow introduces an event-specific dynamic step: the DAF obtained from recorded ground motions is associated with building height through the empirical period-height relationship and used to identify the storey classes to be inspected first. Its practical advantage is therefore not the production of an alternative vulnerability score, but the rapid conversion of available accelerometric records into spatial priorities that can be queried and mapped through the DBMS and GIS.

A limitation of the method concerns the spatial representativeness of the available accelerometric records. Each recording reflects the combined effects of the seismic source, the propagation path, and the local site conditions at the station location and may therefore not fully reproduce the ground motion affecting every building or urban sector. Although stations located closer to the investigated urban areas may provide a more locally significant reference, proximity alone does not exclude differences caused by epicentral distance or local site amplification and was therefore not used as a quantitative weighting criterion. Nevertheless, the availability of permanent stations operating continuously represents a substantial operational advantage, because it allows the method to use ground motions actually recorded during the seismic event. A denser network of free-field stations within the investigated urban areas would improve the spatial resolution and local representativeness of future applications.

Additional uncertainty arises from the rapid exterior survey, the empirical estimation of the building period, the use of discrete representative heights, record-to-record variability, and the idealisation of each building as an equivalent single-degree-of-freedom oscillator. Because the adopted period-height relationship depends only on building height, it does not explicitly account for variations in masonry type, wall arrangement, floor and roof diaphragm stiffness, structural irregularity, or previous strengthening interventions. These characteristics may modify the actual fundamental period and therefore affect the correspondence between the period inferred from height and the spectral-demand range assigned to an individual building. The relationship is consequently appropriate for preliminary urban-scale screening, but not for building-specific dynamic assessment. These uncertainties were not propagated probabilistically in the present study. Consequently, the resulting classes must be interpreted as event-specific screening priorities rather than as deterministic vulnerability or damage predictions. The use of three representative heights per class and the separate processing of all available station–event records provide only a preliminary representation of height and record variability. Future work should quantify the sensitivity of the identified classes to the coefficients α and β, the assumed storey heights, and ground-motion selection, as well as the sensitivity of the spectral amplitudes to the damping ratio, and should propagate these uncertainties through the complete workflow.

4. Conclusions

The proposed method reduces on-site survey times by allowing, with relatively modest hardware and software tools, the immediate recording of the geometric and structural information of the building stock.

Data uploading into the DBMS is automatic and does not alter the structure or integrity of the acquired information. Consequently, subsequent queries, facilitated by the SQL, can be carried out without specific preliminary preprocessing operations.

Calculation of the DAF and identification of the corresponding heights, or critical storeys, consist of simple numerical operations and do not require particular software or hardware resources. The availability of regional numerical cartography also supports the survey phase and completes the subsequent mapping phase.

Therefore, after a survey characterized by an average productivity of approximately 300 buildings per day, it is possible to identify and map, across entire municipalities or densely populated urban areas, masonry buildings to be assigned higher priority in a preliminary screening phase, according to their height and the spectral amplification ratios derived from the recorded ground motions.

The limitations of the method lie in the fact that only one geometric parameter, namely height, is considered. Although this parameter provides useful indications in relation to the dynamic response, it is not sufficient to describe the overall vulnerability of the building. The latter also depends on construction quality, structural details, regularity, state of conservation, ground conditions, and interaction with adjacent buildings.

With reference to the case study, the processed accelerometric records identified Classes I, II and III, corresponding to one-, two- and three-storey masonry buildings. For the illustrative GIS application, the cartographic representation was limited to Classes II and III. Twenty-seven of the 33 damaged masonry buildings included in the preliminary comparison (82%) belonged to these two classes; 22 buildings (67%) showed low or medium damage, and 15 buildings (45%) were constructed between 1945 and 1990. Since these percentages describe the distribution within the damaged-building sample and are not normalised by the total number of buildings belonging to each storey class, the comparison must be interpreted as preliminary and application-based. It nevertheless illustrates how the relationship between building height and the spectral amplification ratios derived from the recorded ground motions can be used as an operational criterion for preliminary spatial prioritisation, without excluding the Class I results produced by the model or replacing subsequent structural assessments.

The comparison between the proposed method and consolidated RVS approaches, as well as with territorial vulnerability approaches reported in the literature, highlights its integrative character. In particular, the method makes it possible to rapidly combine geometric, cartographic, and local accelerometric data, obtaining a first spatial prioritization of masonry buildings. It does not replace comprehensive seismic vulnerability assessment procedures, but may constitute a decision-support tool to be used alongside complete RVS procedures, post-event inspections, and detailed structural analyses.

Supplementary Materials: The following supporting information can be downloaded at: https://www.mdpi.com/article/10.3390/app16168254/s1, BUILDING_DAMAGED.csv: dataset of the 36 buildings recorded as damaged during the rapid survey; DAMAGE.csv: damage-class lookup table; EARTHQUAKE.csv: the three events of the 9 March 2023 seismic sequence; STATION.csv: the seven seismic recording stations considered in the study; ADMINISTRATION.csv: the authorities managing the RAN and RSN networks; STATION_EARTHQUAKE.csv: the 15 station–event records processed in the study; MUNICIPALITY.csv and PROVINCE.csv: territorial lookup tables; DATA_DICTIONARY.csv: field descriptions, units, formats, and notes; README_EN.txt: description of the supplementary data package.

Funding: This research received no external funding.

Data Availability Statement: The Supplementary Materials include UTF-8 CSV exports of the selected relational tables supporting the case study: the dataset of the 36 buildings recorded as damaged, comprising the 33 masonry buildings used in the numerical comparison and the three reinforced-concrete buildings excluded from it; the damage-classification table; the three seismic events; the seven recording stations; and the station–event relationships for the 15 accelerometric records analysed. A data dictionary is also provided. The original accelerometric records are available from the institutional repositories of INGV and the Italian Department of Civil Protection, while the original cartographic data are available from the Umbria Region.

Acknowledgments: The author thanks the Department of Civil Protection and the National Institute of Geophysics and Volcanology for making available the accelerometric data from the seismic stations of Gubbio Piana (GBP), Umbertide (UMB and UMBT), Monte Urbino (MURB), Valfabbrica (VLFB), Montelovesco (ATLO), and Pietralunga (PTL). Special thanks are extended to the students who contributed to the rapid visual survey of the buildings and to the identification of the damaged buildings.

Conflicts of Interest: The author declare no conflict of interest.

Appendix A. Detailed Database Structure and Data Dictionaries

This appendix provides the complete structure of the fields and data dictionaries associated with the tables described in Section 2.2.

Appendix A.1. BUILDING Table

The BUILDING table consists of the following alphanumeric fields:

- ID_Building;
- ID_Map_Building;
- ID_Municipality;
- ID_Province;
- Date of survey;
- Sketch;
- Year of construction or presumed age;
- Use;
- Structural interventions subsequent to the year of construction;
- Building context;
- Planimetric geometry;
- Height;
- Number of storeys above ground;
- Planimetric eccentricities;
- Height eccentricities;
- Thinness;
- Loads distribution;
- Walls;
- Roof geometry;
- Horizontal load-bearing structures;
- Roof load-bearing structures;
- Staircases;
- Elevators;
- Degradation;
- Damage mechanisms—Walls;
- Damage mechanisms—Floors and Roofs;
- Notes;
- ID_Damage.

Some of these fields are associated with data dictionaries that can be selected during the survey through drop-down menus.

Use:

- Residential;
- Industrial;
- Artisanal;
- Agricultural;
- Public;
- Other.

Structural interventions subsequent to the year of construction:

- Expansion;
- Elevation;
- Replacement of floors;
- Replacement of roofs;
- Nothing;
- Other.

Building context:

- Regularity;
- Irregularity;
- Other;

Planimetric geometry:

- Square;
- Rectangular;
- Irregular;
- Other.

Planimetric eccentricities:

- Yes;
- No.

Height eccentricities:

- Yes;
- No.

Thinness:

- Yes;
- No.

Load distribution:

- Regularity;
- Irregularity;
- Other.

Walls:

- Masonry—dry rough-hewn stone;
- Masonry—unbaked bricks;
- Masonry—wet rough-hewn stone;
- Masonry—large stone for monumental constructions;
- Masonry—shaped stone;
- Masonry—brickwork and high-stiffness floor assemblies;
- Masonry - reinforced concrete;
- Other.

Roof geometry:

- Flat;
- One-pitched;
- Dual-pitched;
- Four-pitched;
- Other.

Horizontal load-bearing structures:

- Wooden floors;
- Wood and brick floors;
- Steel and brick floors;
- Reinforced concrete floors;
- Other.

Roof load-bearing structures:

- Wooden roofs;
- Wood and brick roofs;
- Steel and brick roofs;
- Reinforced concrete roofs;
- Other.

Staircases:

- Yes;
- No.

Elevators:

- Yes;
- No.

Degradation:

- Detachment of plaster, coverings;
- Falling tiles;
- Falling cornices, parapets;
- Falling internal or external objects;
- Other.

Damage mechanisms—Walls
Parallel plan:

- Flexural;
- Sliding shear;
- Shear;
- Crushing;
- Other;
- Absent.

Normal plan:

- Overturning simple;
- Overturning partial;
- Overturning composite;
- Other;
- Absent.

Damage mechanisms—Floors and Roofs:

- Thrusting roofs;
- Thrusting and hammering of the roof near the openings;

- Ridge beam hammering;
- Rigid connections at the top associated with poorly resistant elements on the façade;
- Floor detachments/displacements;
- Others;
- Absent.

Appendix A.2. STATION Table

The STATION table consists of the following fields:

- ID_Station;
- ID_Administration;
- Network;
- Full name;
- Name;
- Code;
- Latitude (decimal degree);
- Longitude (decimal degree);
- Elevation (m a.s.l.);
- Notes.

Appendix A.3. ADMINISTRATION Table

The ADMINISTRATION table consists of the following fields:

- ID_Administration;
- Full Name;
- Name;
- Street;
- City;
- Notes.

Appendix A.4. EARTHQUAKE Table

The EARTHQUAKE table consists of the following fields:

- ID_Earthquake;
- Date;
- Time;
- Hypocentre;
- Province;
- Latitude;
- Longitude;
- Depth;
- Magnitude ML;
- Notes.

Appendix A.5. PERIOD AMPLITUDE DAF HEIGHT/STOREY Table

The PERIOD AMPLITUDE DAF HEIGHT/STOREY table consists of the following fields:

- ID_Station;
- ID_Earthquake;
- Period;
- PGA;
- DAF;
- Critical height;

- Critical storey;
- Notes.

Appendix A.6. DAMAGE Table

The DAMAGE table consists of the following fields:

- ID_Damage;
- Type;
- Value;
- Full description;
- Alphanumeric notes.

The numerical damage classification associated with these fields is reported in Table 1 of Section 2.2.

Appendix A.7. Connection Tables

STATION EARTHQUAKE table

The STATION EARTHQUAKE table is the many-to-many connection table between the STATION table and the EARTHQUAKE table. Its fields are:

- ID_Earthquake;
- ID_Station.

BUILDING EARTHQUAKE table

The BUILDING EARTHQUAKE table is the many-to-many connection table between the BUILDING table and the EARTHQUAKE table. Its fields are:

- ID_Building;
- ID_Earthquake.

References

1. NTC. Technical regulations for buildings. *Official Document of the Italian Government n° 42*, 20 February 2018. (In Italian)
2. *OPCM 3274*; Primi Elementi in Materia di Criteri Generali per la Classificazione Sismica del Territorio Nazionale e di Normative Tecniche per le Costruzioni in Zona Sismica. Official Document of the Italian Government n° 105. Presidency of the Council of Ministers: Rome, Italy, 2003. (In Italian)
3. Ademović, N.; Kalman Šipoš, T.; Hadzima-Nyarko, M. Rapid assessment of earthquake risk for Bosnia and Herzegovina. *Bull. Earthq. Eng.* **2020**, *18*, 1835–1863. [CrossRef]
4. Albayrak, U.; Canbaz, M.; Albayrak, G. A rapid seismic risk assessment method for existing building stock in urban areas. *Procedia Eng.* **2015**, *118*, 1242–1249. [CrossRef]
5. Šipoš, T.K.; Hadzima-Nyarko, M. Rapid seismic risk assessment. *Int. J. Disaster Risk Reduct.* **2017**, *24*, 348–360. [CrossRef]
6. FEMA Federal Emergency Management Agency. *Multi-Hazard Loss Estimation Methodology—Earthquake Module: HAZUS-MHMR1 Advanced Engineering Building Module Technical and User's Manual*, 3rd ed.; Federal Emergency Management Agency: Washington, DC, USA, 2003.
7. FEMA Federal Emergency Management Agency. *Rapid Visual Screening of Buildings for Potential Seismic Hazards: A Handbook FEMAP-154*, 3rd ed.; Applied Technology Council (ATC), Federal Emergency Management Agency: Washington, DC, USA, 2015.
8. FEMA Federal Emergency Management Agency. *Rapid Visual Screening of Buildings for Potential Seismic Hazards: Supporting Documentation FEMAP-155*, 3rd ed.; Applied Technology Council (ATC), Federal Emergency Management Agency: Washington, DC, USA, 2015.
9. Rai, D.C. *Review of Documents on Seismic Evaluation of Existing Buildings*; Department of Civil Engineering, Indian Institute of Technology Kanpur: Kanpur, India, 2005; IITK-GSDMA-EQ03-V1.0:1-32.
10. Dolce, M.; Prota, A.; Borzi, B.; Da Porto, F.; Lagomarsino, S.; Magenes, G.; Moroni, C.; Penna, A.; Polese, M.; Speranza, E.; et al. Seismic risk assessment of residential buildings in Italy. *Bull. Earthq. Eng.* **2021**, *19*, 2999–3032. [CrossRef]
11. World Bank Gpurl D-Ras Team. *M 6.4 Albania Earthquake Global Rapid Post Disaster Damage Estimation (Grade) Report*; International Bank for Reconstruction and Development/The World Bank: Washington DC, USA, 2019; Volume 20433, pp. 1–31.
12. Boutaraa, Z.; Caterina, N.; Ahmed, A.; Olivier, S. Buildings vulnerability assessment and damage seismic scenarios at urban scale: Application to Chlef City (Algeria). *J. Civ. Eng.* **2018**, *22*, 3948–3960. [CrossRef]

13. Khemis, A.; Athmani, A.; Ademović, N. Rapid application of the RISK-UE LM2 method for the seismic vulnerability analysis of the Algerian masonry buildings. *Int. J. Archit. Herit.* **2023**, *18*, 788–808. [CrossRef]
14. Ademović, N.; Hadzima-Nyarko, M.; Zagora, N.; Piljug, A.; Medanović, Ć. Vulnerability of Residential Buildings in Sarajevo. In *Advanced Technologies, Systems, and Applications VII Proceedings of the International Symposium on Innovative and Interdisciplinary Applications of Advanced Technologies (IAT), Sarajevo, Bosnia and Herzegovina, 23–26 June 2022*; Lecture Notes in Networks and Systems; Springer: Cham, Switzerland, 2022; pp. 3–14.
15. Fathi-Fazl, R.; Fazileh, F.; Cai, Z.; Cortés-Puentes, W.L. Development of quick seismic evaluation procedure for existing buildings in Canada. *Can. J. Civ. Eng.* **2023**, *50*, 408–422. [CrossRef]
16. Ward, H.S. *Earthquake Load Provisions of the National Building Code of Canada*; National Research Council of Canada. Division of Building Research: Ottawa, ON, Canada, 1966; Volume 1966, pp. 1–26.
17. JBDPA Japan Building Disaster Prevention Association. *Seismic Evaluation and Retrofit*; JBDPA: Tokyo, Japan, 2001.
18. EPPO. *Post-Earthquake Damage Inspection of Buildings: Guidelines and Forms for Post-Earthquake Damage Surveys*; Earthquake Planning and Protection Organization: Athens, Greece, 1984.
19. EPPO. *Instructions and Forms for Post-Earthquake Usability Assessment of Buildings*; Earthquake Planning and Protection Organization: Athens, Greece, 1997.
20. EPPO. *Provisions for Pre-Earthquake Vulnerability Assessment of Public Buildings*; Earthquake Planning and Protection Organization: Athens, Greece, 2000.
21. Pomonis, A.; Gaspari, M.; Karababa, F. Seismic vulnerability assessment for buildings in Greece based on observed damage data sets. *Boll. Geofis. Teor. Appl.* **2012**, *54*, 1–34.
22. TDMRC (Tsunami Disaster Mitigation Research Center). *Report on Disaster Risk Maps for Aceh (Tsunami Earthquake Landslides Floods)*; TDMRC: Banda Aceh, Indonesia, 2019.
23. NZSEE New Zealand Society for Earthquake Engineering. Assessment and Improvement of the Structural Performance of Buildings in Earthquakes. In *Recommendations of a NZSEE Study Group on Earthquake Risk Buildings*; NZSEE New Zealand Society for Earthquake Engineering: Wellington, New Zealand, 2006; pp. 1–388.
24. Sarmaha, T.; Dasab, S. Earthquake vulnerability assessment for RCC buildings of Guwahati City using rapid visual screening. *Procedia Eng.* **2018**, *212*, 214–221. [CrossRef]
25. Ornthammarath, T.; Warnitchai, P.; Worakanchana, K.; Zaman, S.; Sigbjörnsson, R.; Lai, C.G. Probabilistic seismic hazard assessment for Thailand. *Bull. Earthq. Eng.* **2011**, *9*, 367–394. [CrossRef]
26. Palasri, C.; Ruangrassamee, A. Probabilistic seismic hazard maps of Thailand. *J. Earthq. Tsunami.* **2010**, *4*, 369–386. [CrossRef]
27. Warnitchai, P.; Sangarayakul, C.; Ashford, S.A. Seismic hazard in Bangkok due to distant earthquakes. In Proceedings of the 2nd Multi-lateral Workshop on Development of Earthquake and Tsunami Disaster Mitigation Technologies and Their Integration for the Asia-Pacific Region, Kobe, Japan, 1–2 March 2000.
28. Vallejo, C.B. Rapid visual screening of buildings in the city of Manila, Philippines. In *Proceedings of 5th Civil Engineering Conference in the Asian Region and Australasian Structural Engineering Conference, Sydney, Australia, 8–12 August 2010*; Engineers Australia: Sydney, NSW, Australia, 2010; pp. 510–518.
29. Ansal, A.; Özaydın, K.; Edinçliler, A.; Sağlamer, A.; Sucuoğlu, H.; Özdemir, P. *Earthquake Master Plan for Istanbul. Metropolitan Municipality of Istanbul Planning and Construction Directorate*; Geotechnical and Earthquake Investigation Department: Istanbul, Turkey, 2003; pp. 1–568.
30. Askan, A.; Yucemen, M.; Semih, A. Probabilistic methods for the estimation of potential seismic damage: Application to reinforced concrete buildings in Turkey. *Struct. Saf.* **2010**, *32*, 262–271. [CrossRef]
31. Işık, E.; Ulu, A.E.; Büyüksaraç, A.; Aydin, M.C. A study on damages in masonry structures and determination of damage levels in the 2020 Sivrice (Elazig) earthquake. In *Advanced Technologies, Systems, and Applications VII Proceedings of the International Symposium on Innovative and Interdisciplinary Applications of Advanced Technologies (IAT), Sarajevo, Bosnia and Herzegovina, 23–26 June 2022*; Lecture Notes in Networks and Systems; Springer: Cham, Switzerland, 2022; pp. 26–35.
32. NCRRE National Center for Research on Earthquake Engineering of Taiwan. *NCRR Research*; NAR Labs: Taipei, Taiwan, 2018; Volume 200, pp. 1–144.
33. Falcone, R.; Lima, C.; Martinelli, E. Soft computing techniques in structural and earthquake engineering: A literature review. *Eng. Struct.* **2020**, *207*, 110269. [CrossRef]
34. Ghaboussi, J. *Soft Computing in Engineering*, 1st ed.; CRC Press Taylor & Francis: Boca Raton, FL, USA, 2018; pp. 1–220.
35. Kostinakis, K.; Morfidis, K. Application of Artificial Neural Networks for the Assessment of the Seismic Damage of Buildings with Irregular Infills' Distribution. In *Seismic Behaviour and Design of Irregular and Complex Civil Structures III*; Springer: Cham, Switzerland, 2020; pp. 291–306.
36. Lazaridis, P.C.; Kavvadias, I.E.; Demertzis, K.; Iliadis, L.; Papaleonidas, A.; Vasiliadis, L.K.; Elenas, A. Structural Damage Prediction Under Seismic Sequence Using Neural Networks. In Proceedings of the 8th ECCOMAS Thematic Conference on Computational Methods in Structural Dynamics and Earthquake Engineering, Athens, Greece, 28–30 June 2021.

37. Li, J.; He, Z.; Zhao, X. A data-driven building's seismic response estimation method using a deep convolutional neural network. *IEEE Access* **2021**, *9*, 50061–50077. [CrossRef]
38. Oh, B.K.; Park, Y.; Park, H.S. Seismic response prediction method for building structures using convolutional neural network. *Struct. Control Health Monit.* **2020**, *27*, 2519. [CrossRef]
39. Harirchian, E.; Lahmer, T. Improved rapid visual earthquake hazard safety evaluation of existing buildings using a type-2 fuzzy logic model. *Appl. Sci.* **2020**, *10*, 2375. [CrossRef]
40. Yariyan, P.; Zabihi, H.; Wolf, I.D.; Karami, M.; Amiriyan, S. Earthquake risk assessment using an integrated fuzzy analytic hierarchy process with artificial neural networks based on GIS: A case study of Sanandaj in Iran. *Int. J. Disaster Risk Reduct.* **2020**, *50*, 101705. [CrossRef]
41. Sun, H.; Burton, H.V.; Huang, H. Machine learning applications for building structural design and performance assessment: State-of-the-art review. *J. Build. Eng.* **2020**, *33*, 101816. [CrossRef]
42. Thaler, D.; Stoffel, M.; Markert, B.; Bamer, F. Machine-learning-enhanced tail end prediction of structural response statistics in earthquake engineering. *Earthq. Eng. Struct. Dyn.* **2021**, *50*, 2098–2114. [CrossRef]
43. Xie, Y.; Ebad Sichani, M.; Padgett, J.E.; DesRoches, R. The promise of implementing machine learning in earthquake engineering: A state-of-the-art review. *Earthq. Spectra.* **2020**, *36*, 769–1801. [CrossRef]
44. Vrochidou, E.; Bizergianidou, V.; Andreadis, I.; Elenas, A. Assessment and localization of structural damage in r/c structures through intelligent seismic signal processing. *Appl. Artif. Intell.* **2021**, *35*, 670–695. [CrossRef]
45. Bektaş, N.; Kegyes-Brassai, O. Conventional RVS methods for seismic risk assessment for estimating the current situation of existing buildings: A state-of-the-art review. *Sustainability* **2022**, *14*, 2583. [CrossRef]
46. Harirchian, E.; Hosseini Aghakouchaki, S.E.; Jadhav, K.; Kumari, V.; Rasulzade, S.; Işık, E.; Wasif, M.; Lahmer, T. A review on application of soft computing techniques for the rapid visual safety evaluation and damage classification of existing buildings. *J. Build. Eng.* **2021**, *43*, 102536. [CrossRef]
47. Ji, D.; Wen, W.; Zhai, C.; Katsanos, E.I. Maximum inelastic displacement of mainshock-damaged structures under succeeding aftershock. *Soil Dyn. Earthq. Eng.* **2020**, *136*, 106248. [CrossRef]
48. Yu, X.; Zhou, Z.; Du, W.; Lu, D. Development of fragility surfaces for reinforced concrete buildings under mainshock-aftershock sequences. *Earthq. Eng. Struct. Dyn.* **2021**, *50*, 3981–4000. [CrossRef]
49. Zhou, Z.; Yu, X.; Lu, D. Identifying optimal intensity measures for predicting damage potential of mainshock–aftershock sequences. *Appl. Sci.* **2020**, *10*, 6795. [CrossRef]
50. Bilgin, H.; Shkodrani, N.; Hysenlliu, M.; Ozmen, H.B.; Işık, E.; Harirchian, E. Damage and performance evaluation of masonry buildings constructed in 1970s during the 2019 Albania earthquakes. *Eng. Fail. Anal.* **2021**, *31*, 105824. [CrossRef]
51. Freddi, F.; Novelli, V.; Gentile, R.; Stoyan, E.; Veliu, A.; Andreev, A.; Greco, F.; Zhuleku, E. Observations from the 26th November 2019 Albania earthquake: The earthquake engineering field investigation team (EEFIT) mission. *Bull. Earthq. Eng.* **2021**, *19*, 1–32. [CrossRef]
52. Leti, M.; Bilgin, H. Predicting the Seismic Performance of Typical R/C Residential Buildings. In *Advanced Technologies, Systems, and Applications VII Proceedings of the International Symposium on Innovative and Interdisciplinary Applications of Advanced Technologies (IAT), Sarajevo, Bosnia and Herzegovina, 23–26 June 2022*; Lecture Notes in Networks and Systems; Springer: Cham, Switzerland, 2022; pp. 15–24.
53. Shkodrani, N.; Bilgin, H.; Hysenlliu, M. Influence of interventions on the seismic performance of URM buildings designed according to pre-modern codes. *Res. Eng. Struct. Mater.* **2021**, *7*, 315–330. [CrossRef]
54. Zucconi, M.; Sorrentino, L.; Ferlito, R. Principal component analysis for a seismic usability model of unreinforced masonry buildings. *Soil Dynam. Earthq. Eng.* **2017**, *96*, 64–75. [CrossRef]
55. Abide, A.; Vasconcelos, G.; Lourenco, P.B. Overview on the nonlinear static procedures and performance-based approach on modern unreinforced masonry buildings with structural irregularity. *Buildings* **2021**, *11*, 147. [CrossRef]
56. Kanai, K. Semi-empirical formula for the seismic characteristics of the ground. *Bull. Earthq. Res. Inst.* **1957**, *35*, 309–325.
57. Ozcebe, G.; Yucemen, M.S.; Aydogan, V. Statistical seismic vulnerability assessment of existing reinforced concrete buildings in Turkey on a regional scale. *J. Earthq. Eng.* **2004**, *8*, 749–773. [CrossRef]
58. Balendra, T.; Lam, N.T.K.; Wilson, J.L.; Hau, K.K. Analysis of long-distance earthquake tremors and base shear demand for buildings in Singapore. *Eng. Struct.* **2002**, *24*, 99–108. [CrossRef]
59. Celebi, M. Revelations from a single strong-motion record retrieved during the 27 June 1998 Adana (Turkey) earthquake. *Soil Dyn. Earthq. Eng.* **2000**, *20*, 283–288. [CrossRef]
60. Drimmel, J. A theoretical basis for macroseismic scales and some implications for practical work. *Eng. Geol.* **1984**, *20*, 99–104. [CrossRef]
61. Pan, T.C.; Megawati, K.; Goh, K.S. Response of high-rise buildings in Singapore due to a potential giant earthquake in the Sumatran megathrust. *J. Earthq. Eng.* **2011**, *15*, 90–106. [CrossRef]

62. Du, W.; Goh, K.S.; Pan, T.C. Methodology for estimating human perception to tremors in high-rise buildings. *J. Seismol.* **2017**, *21*, 667–682. [CrossRef]
63. Gatti, M. Relation between dynamic amplification, structural height and damage in buildings affected by the recent Italian earthquakes. *Geomat. Nat. Haz. Risk.* **2020**, *11*, 1154–1174. [CrossRef]
64. Gatti, M. Structural height, amplification and damages during the superficial earthquakes at Casamicciola, Ischia Island (2017), and Santa Venerina, Catania (2018), Italy. *Geomat. Nat. Haz. Risk.* **2023**, *14*, 2182172. [CrossRef]
65. Gatti, M. A rapid method to census the seismic risk class of masonry buildings. *Geomat. Nat. Haz. Risk.* **2024**, *15*, 2361120. [CrossRef]
66. Alam, M.N.; Tesfamariam, S.; Alam, M.S. GIS-based seismic damage estimation: Case study for the City of Kelowna, BC. *Nat. Hazards Rev.* **2013**, *14*, 66–78. [CrossRef]
67. Dou, C.E.; Jia, Y.H.; Xie, H.Q. Construction and information management of Lianyungang emergency shelters for earthquake disaster based on GIS. *Adv. Mater. Res.* **2013**, *610*, 3624–3627. [CrossRef]
68. Fallah-Aliabadi, S.; Ostadtaghizadeh, A.; Ardalan, A.; Eskandari, M.; Fatemi, F.; Mirjalili, M.R.; Khazai, B. Risk analysis of hospitals using GIS and HAZUS: A case study of Yazd County, Iran. *Int. J. Disaster Risk Reduct.* **2020**, *47*, 101552. [CrossRef]
69. Hashemi, M.; Alesheikh, A.A. A GIS-based earthquake damage assessment and settlement methodology. *Soil Dyn. Earthq. Eng.* **2011**, *31*, 1607–1617. [CrossRef]
70. Huang, M.; Zhang, D.; Li, P.; Zhang, Y.; Zhang, R. Study of earthquake disaster prediction system of Langfang city based on GIS. *IOP Conf. Ser. Mater. Sci. Eng.* **2017**, *224*, 012049. [CrossRef]
71. Irwansyah, E. Building damage assessment using remote sensing, aerial photograph and GIS data-case study in Banda Aceh after Sumatera Earthquake 2004. In *Proceedings of the Seminar on Intelligent Technology and Its Application*; SITIA 2010; Zenodo: Geneva, Switzerland, 2010; Volume 11, pp. 57–65.
72. Irwansyah, E.; Hartati, S. Assessment of building damage hazard caused by earthquake: Integration of FNN and GIS. *IERI Procedia* **2014**, *10*, 196–202. [CrossRef]
73. Jefferson, T.L.; Johannes, T.W. Using geographic information systems to support decision making in disaster response. *Intell. Decis. Technol.* **2016**, *10*, 193–207. [CrossRef]
74. Yang, K.; Xu, Q.-L.; Peng, S.-Y.; Cao, Y.-B. The design and implementation of urban earthquake disaster loss evaluation and emergency response decision support systems based on ArcGIS. In *Proceedings of the IEEE International Symposium on Geoscience and Remote Sensing, Denver, CO, USA, 31 July 2006–4 August 2006*; IEEE: New York, NY, USA, 2006; pp. 892–895.
75. Leggieri, V.; Mastrodonato, G.; Uva, G. GIS multisource data for the seismic vulnerability assessment of buildings at the urban scale. *Buildings* **2022**, *12*, 523. [CrossRef]
76. Liebenberg, K.; Smit, A.; Coetzee, S.; Kijko, A. A GIS approach to seismic risk assessment with an application to mining-related seismicity in Johannesburg, South Africa. *Acta Geophys.* **2017**, *65*, 645–657. [CrossRef]
77. Mussumeci, G.; Falchi, U.; Condorelli, A. Data survey and management techniques in civil protection emergencies. In Proceedings of the XXth Congress of International Society of Photogrammetry and Remote Sensing (ISPRS), Istanbul, Turkey, 12–23 July 2004.
78. Peng, S.Y.; Yang, K. The design and development of an earthquake rapid assessment system based on GIS technology in Yunnan. *Adv. Mater. Res.* **2014**, *926*, 2590–2593. [CrossRef]
79. Sauti, N.S.; Daud, M.E.; Kaamin, M.; Sahat, S. GIS spatial modelling for seismic risk assessment based on exposure, resilience, and capacity indicators to seismic hazard: A case study of Pahang, Malaysia. *Geomat. Nat. Haz. Risk.* **2021**, *12*, 1948–1972. [CrossRef]
80. Senouci, A.; Bard, P.Y.; Beck, E.; Farsi, M.N.; Cartier, S. Mapping seismic vulnerability at urban scale: Discussion on relevant cartography representations and smoothing for urban planning purposes on the Oran case study. *Soil Dyn. Earthq. Eng.* **2018**, *115*, 545–563. [CrossRef]
81. Zhai, Y.; Chen, S.; Ouyang, Q. GIS-based seismic hazard prediction system for urban earthquake disaster prevention planning. *Sustainability* **2019**, *11*, 2620. [CrossRef]
82. Işık, E. *Structural failures of adobe buildings during the February* 2023 Kahramanmaraş (Türkiye) earthquakes. *Appl. Sci.* **2023**, *13*, 8937. [CrossRef]
83. Arkan, E.; Işık, E.; Harirchian, E.; Topçubaşı, M.; Avcil, F. Architectural characteristics and determination seismic risk priorities of traditional masonry structures: A case study for Bitlis (Eastern Türkiye). *Buildings* **2023**, *13*, 1042. [CrossRef]
84. Arkan, E.; Işik, E.; Avcil, F.; İzol, R.; Büyüksaraç, A. Seismic damages in masonry structural walls and solution suggestions. *Acad. Platf. J. Nat. Hazards Disaster Manag.* **2023**, *4*, 49–64. [CrossRef]
85. Işık, E.; Avcil, F.; Büyüksaraç, A.; İzol, R.; Arslan, M.H.; Aksoylu, C.; Harirchian, E.; Eyisüren, O.; Arkan, E.; Güngür, M.Ş.; et al. Structural damages in masonry buildings in Adıyaman during the Kahramanmaraş (Turkiye) earthquakes (Mw 7.7 and Mw 7.6) on 06 February 2023. *Eng. Fail. Anal.* **2023**, *151*, 107405. [CrossRef]
86. Collettini, C.; Barchi, M.R.; Chiaraluce, L.; Mirabella, F.; Pucci, S. The Gubbio fault: Can different methods give pictures of the same object? *J. Geodyn.* **2003**, *36*, 51–66. [CrossRef]
87. Codd, E.F. A relational model of data for large shared data banks. *Commun. ACM.* **1970**, *13*, 377–387. [CrossRef]

88. Codd, E.F. *Relational Completeness of Data Base Sublanguages*; IBM Research Laboratory: San Jose, CA, USA, 1972; pp. 65–98.
89. Codd, E.F. Further normalization of the data base relational model. *Data Base Syst.* **1972**, *6*, 33–64.
90. Boore, D.M.; Akkar, S. Effects of causal and acausal filters on elastic and inelastic response spectra. *Earthq. Eng. Struct. Dyn.* **2003**, *32*, 1729–1748. [CrossRef]
91. Lynn, P.A.; Fuerst, W. *Introductory Digital Signal Processing with Computer Applications*; Wiley & Sons: Hoboken, NJ, USA, 1998.
92. Stearns, S.; David, R. *Signal Processing Algorithms*; Prentice-Hall: Englewood Cliffs, NJ, USA, 1996.
93. Gatti, M. Peak horizontal vibrations from GPS response spectra in the epicentral areas of the 2016 earthquake in central Italy. *Geomat. Nat. Haz. Risk.* **2018**, *9*, 403–415. [CrossRef]
94. Jeary, A.P. Damping in tall buildings. A mechanism and a predictor. *Earthq. Eng. Struct. Dyn.* **1986**, *14*, 733–750. [CrossRef]
95. ESDU—Engineering Sciences Data Unit. *Structural Parameters Used in Response Calculations (Estimation of Numerical Values)*; ESDU—Engineering Sciences Data Unit: London, UK, 1991; ESDU International Item N. 91001.
96. Chopra, A.K. *Dynamics of Structures: Theory and Applications to Earthquake Engineering*; Prentice-Hall, Inc.: Upper Saddle River, NJ, USA, 1995.
97. Fang, J.Q.; Li, Q.S.; Jeary, A.P.; Liu, D.K. Damping of tall buildings: Its evaluation and probabilistic characteristics. *Struct. Des. Tall Spec.* **1999**, *8*, 145–153. [CrossRef]
98. Satake, N.; Suda, K.; Arakawa, T.; Sasaki, A.; Tamura, Y. Damping evaluation using full scale data of buildings in Japan. *J. Struct. Eng.* **2003**, *129*, 470–477. [CrossRef]
99. Lin, Y.Y.; Miranda, E.; Chang, K.C. Evaluation of damping reduction factors for estimating elastic response of structures with high damping. *Earthq. Eng. Struct. Dyn.* **2005**, *34*, 1427–1443. [CrossRef]
100. Elnashai, A.S.; Di Sarno, L. *Fundamentals of Earthquake Engineering*; John Wiley & Sons: Chichester, UK, 2008.
101. Gatti, M. Experimental calculation of the damping ratio in buildings hosting permanent GPS stations during the recent Italian earthquakes. *Adv. Civ. Eng. Tech.* **2018**, *1*, 1–20. [CrossRef]
102. ATC Applied Technological Council. *Tentative Provisions for the Development of Seismic Regulations for Buildings*; ATC3-06; Applied Technological Council: Palo Alto, CA, USA, 1978.
103. Goel, R.K.; Chopra, A.K. Period formulas for moment-resisting frame buildings. *J. Struct. Eng.* **1997**, *123*, 1454–1461. [CrossRef]
104. SEAOC. *Recommended Lateral Force Requirements and Commentary*; Seismological Engineers Association of California: San Francisco, CA, USA, 1996.
105. Hong, L.; Hwang, W. Empirical formula for fundamental vibration periods of reinforced concrete buildings in Taiwan. *Earthq. Eng. Struct. Dyn.* **2000**, *29*, 327–333. [CrossRef]
106. CEN. *European Prestandard ENV 1998-1-4: Eurocode 8—Design of Structures for Earthquake Resistance, Part 1–4: Strengthening and Repair of Buildings*; Comité Européen de Normalisation: Brussels, Belgium, 2004.
107. ISTAT. Permanent Census of Population and Housing. 2018. Available online: https://www.istat.it/it/censimenti-permanenti/ (accessed on 11 June 2023).
108. SIAT. *Regional Environmental and Territorial Information System Umbria Region*; Regione Umbria: Perugia, Italy, 2019.
109. Bolt, B.A. Duration of strong ground motion. In *Proceedings of the 5th World Conference on Earthquake Engineering, Rome, Italy, 25–29 June 1973*; EDIGRAF (Editrice Libraria): Rome, Italy, 1973; Volume 1, pp. 1304–1313.
110. Du, W.; Wang, G. Prediction equations for ground motion significant durations using the NGA-West2 database. *Bull. Seismol. Soc. Am.* **2017**, *107*, 319. [CrossRef]
111. Trifunac, M.D.; Brady, A.G. A study on the duration of strong earthquake ground motion. *Bull. Seism. Soc. Am.* **1975**, *65*, 581–626.

Disclaimer/Publisher's Note: The statements, opinions and data contained in all publications are solely those of the individual author(s) and contributor(s) and not of MDPI and/or the editor(s). MDPI and/or the editor(s) disclaim responsibility for any injury to people or property resulting from any ideas, methods, instructions or products referred to in the content.